A new lidar for water vapor and temperature measurements in the Atmospheric Boundary Layer

M. Froidevaux[1], I. Serikov[2], S. Burgos[3], P. Ristori[1], V. Simeonov[1], H. Van den Bergh[1], and M.B. Parlange[1]

[1]Swiss Federal Institute of Technology at Lausanne (EPFL) - School of Architecture, Civil and Environmental Engineering
[2]Max Planck Institute for Meteorology, Hamburg, Germany
[3]Changins Engineering School, Nyon, Switzerland

Introduction

Processes governing weather and climate at the large scale are affected by turbulent interactions at the land-atmosphere interface. To understand and better predict the exchange of water and heat at the earth's surface, the distribution of temperature and water vapor in the lower atmosphere must be accurately measure both in space and in time, and at a range of scales. To investigate these land-atmosphere interactions at small scales, a new lidar (Light Detection and Ranging) was designed and constructed. This new generation lidar is based on the Raman scattering effect and is capable of providing simultaneous high resolution measurements of temperature and water vapor, from distances of 15 to 500 meters, measuring every meter and every second, day and night. It provides an unprecedented view of the spatial and temporal variability of these scalars. The operating principle and design of the EPFL Raman lidar and some profiles of water vapor taken above the EPFL campus is presented here, as well as the results from the first real outdoor test experiment, which took place over a vineyard, close to Geneva, Switzerland, from September 6th to 12th, 2007.

EPFL Raman lidar principle

The EPFL Raman lidar is based on the same basic principle as other active remote sensing techniques (radar, sonar, sodar), in which the instrument transmits a short electromagnetic or acoustic pulse and then detects and analyzes the response from the fluid. The light pulse is emitted from a quadrupled nd:YAG laser at 266 nm. This wavelength is in the UV range known as the "solar-blind" region (wavelengths shorter than 300 nm) because practically all radiation at these wavelengths is absorbed by the ozone layer in the stratosphere. It gives the advantage that there is no daytime solar background radiation in the system (Renaut, Pourny et al. 1980; Grant 1991). During its propagation through the atmosphere, the pulse of light is scattered and spreads out or backscatters, as it encounters various molecules in the air. Because the laser pulse is very short, only a certain volume gives a backscatter response at a given time. The measurements thus have a spatial resolution that is defined by the laser pulse duration. The radiation that is scattered back towards the receiver contains information on atmospheric properties and the spectrum of the scattered radiation has several important features. The spectrum of the Raman lines used by the lidar is presented in Fig. 1. The "elastic line" has the same wavelength as that of the laser. "Raman lines" are wavelengths shifted from the elastic line. Each wavelength shift is specific for a particular scattering molecule, and the scattering intensity is a function of molecule concentration and temperature. The pure rotational Raman lines surrounding the elastic line are temperature sensitive, and are used for temperature

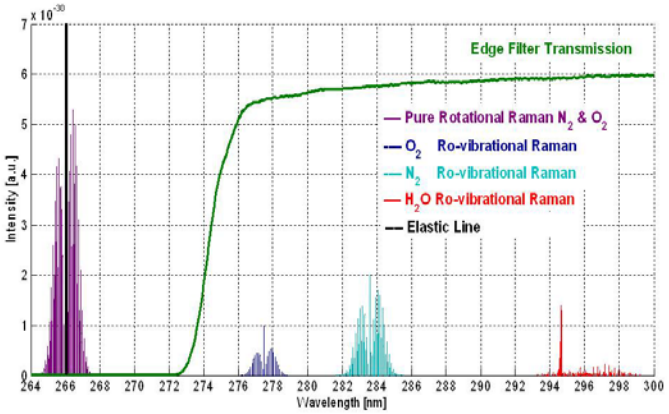

Figure 1. spectroscopic principle

measurements (Arshinov, Bobrovnikov et al. 1983; Mattis, Ansmann et al. 2002). The water vapor concentration is derived from the ratio of water vapor to nitrogen ro-vibrational Raman lines (Whiteman, Melfi et al. 1992). The oxygen ro-vibrational Raman lines are used for alignment purposes and tropospheric ozone correction. The initial spectral separation between "temperature" and "water vapor" signals is done with an edge filter; its transmission is also shown in green on Fig. 1. Two different optical analyzers called polychromators are used for the final spectral analysis of these two parts of the spectrum.

Lidars usually collect the backscattered light with a single mirror telescope. A major issue is that the amount of collected light is proportional to the mirror's area and inversely proportional to the square of the distance to the scattering volume. Thus, the accuracy decreases

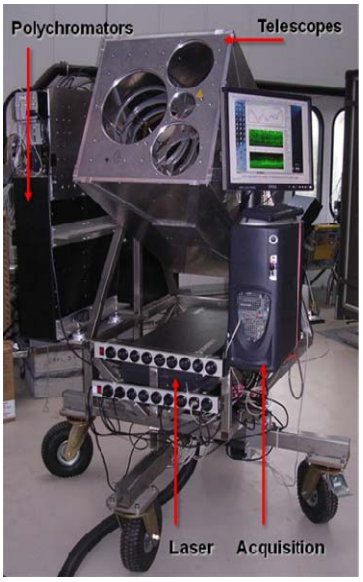

Figure 2. EPFL Raman lidar

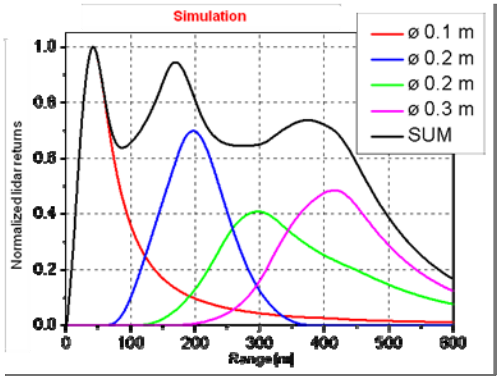

Figure 3. telescopes overlap

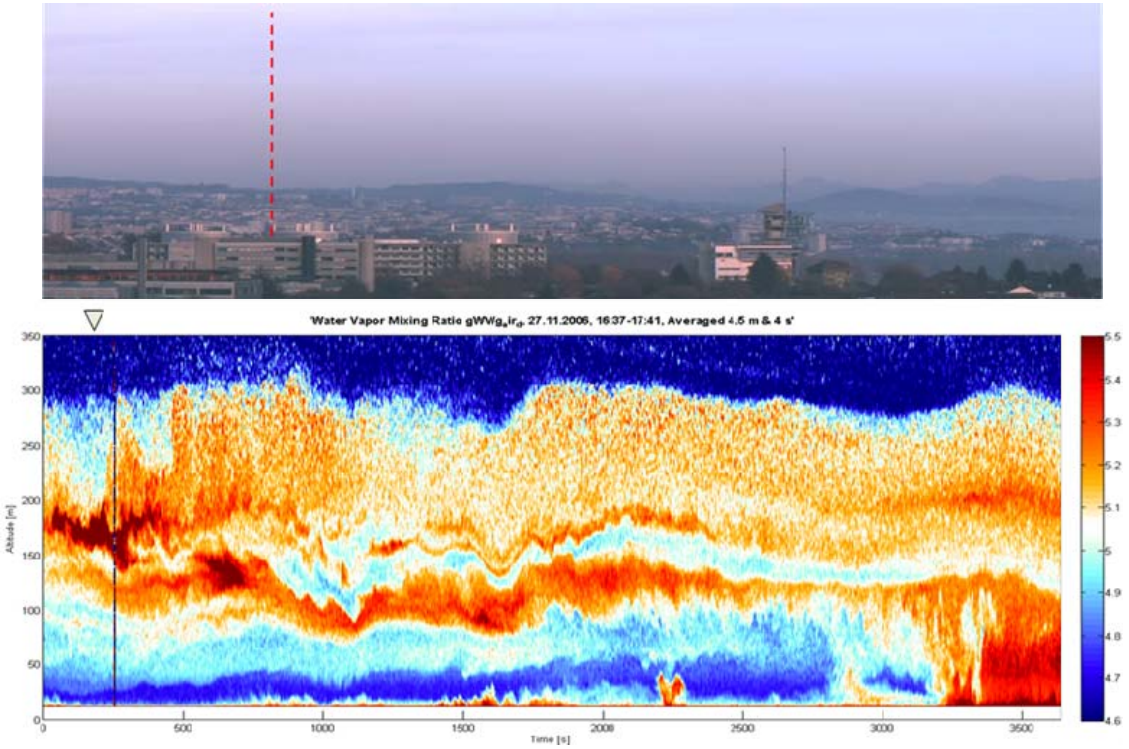

Figure 4. site view and vertical evolution of the water vapor mixing ratio

rapidly as distance from the receiver increases. By introducing a design (Fig. 2) that uses four receiving telescopes instead of one, an almost range-independent signal over its entire operational range (15-500 m) is obtained (Fig. 3) giving us measurements with almost constant spatial and temporal resolution and accuracy.

Vertical profiles

One of the first test measurements of water vapor was done on November 27th 2006, between 16:37 and 17:41 local time, on the EPFL campus, during calm weather conditions with light fog. This high resolution image (fig. 4) gives us an idea of the variability of water vapor, even in calm weather conditions. A clear double layer of water vapor, which collapsed to the ground after sunset at the end of the measurements period can be observed.

Vineyard test experiment

The first real outdoor test experiment carried out with the EPFL Raman lidar was made above a vineyard parcel (100x150m), equipped with two eddy covariance towers. Four temperature and humidity point sensors mounted on a Sensorscope wireless local network was also used, set in a line right below the principal line of sight of the lidar. A top view of the site and the instrumental configuration is shown in Fig. 5. The purpose of the vineyard experiment was first to compare lidar data with simultaneous point-sensor measurements at different horizontal distances. This showed that the multi-faced design telescope is reliable. We also could estimate the accuracy of the measurements; 0.15 g/kg for water vapor and 0.3°K for temperature, with 60 seconds averaging. One hour and a half time series comparison of lidar data and sensor is shown in Fig. 6. The first sensor has a small shift because this sensor was too much below the lidar beam, due to a small terrain depression. The usual estimation of lidar precision with Poisson statistics overestimates the real noise present in our profiles. The

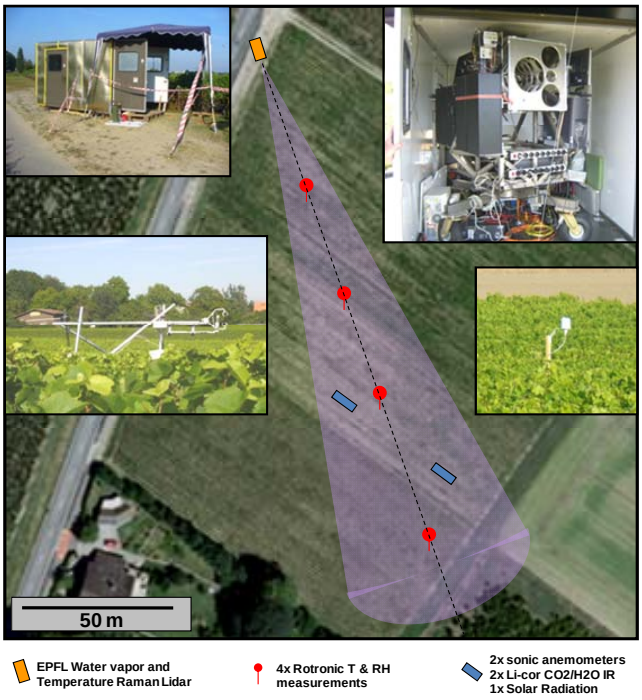

Figure 5. Top view of the experimental site

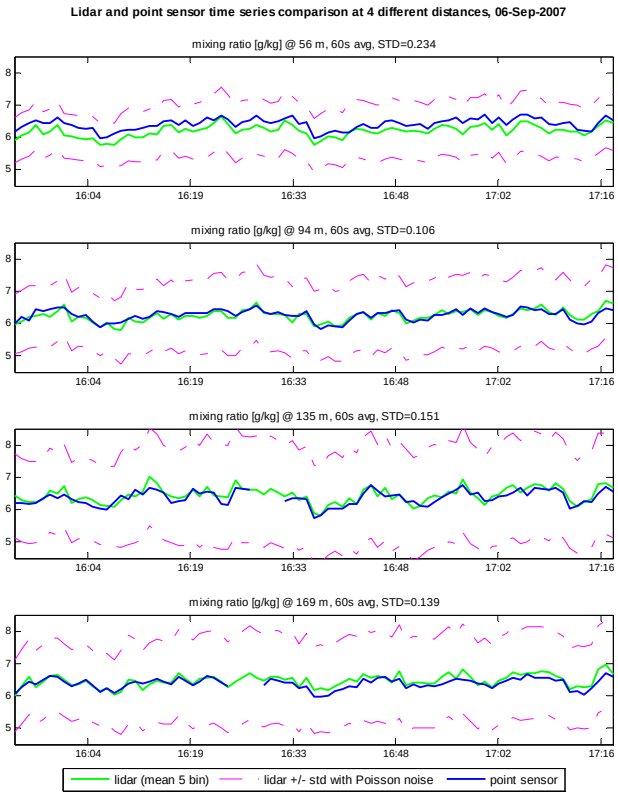

Figure 6. lidar and point sensor mixing ratio comparison

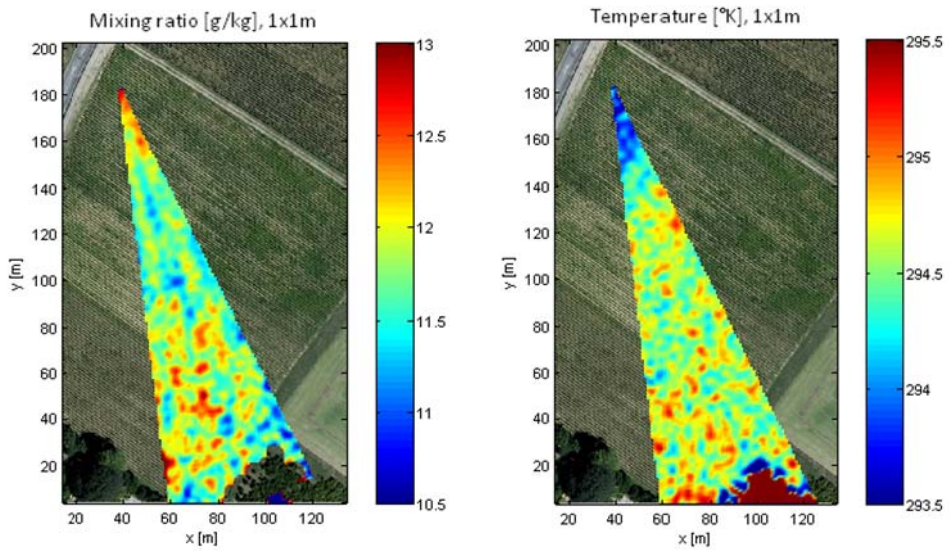

Figure 7. Mixing ratio (left) and Temperature scan (right)

second objective was to observe spatial structures of water vapor and temperature right above a plant canopy by scanning the air horizontally and vertically. The horizontal water vapor scans have complex footprints and source regions are not easy to determine, even if the sounding beam was within one meter of the vegetation. An example of one horizontal scan is shown in Fig. 7, with a pixel resolution of 1x1m and smoothed with a moving average of 4x4 m.

The horizontal temperature field is more variable than water vapor, which contains larger structures. This observation can be explained by the fact that temperature variations are quite large between the shaded and the exposed side of a vineyard line to the sun and could enhance the small-scales buoyancy effects.

The vertical scans were the most informative. A vertical resolution of 0.2 m was obtained by scanning at ~1°/min. The mean of 17 consecutive scans is presented in Fig. 8. During these measurements, the wind was between 0.5 and 1.5 m/s and mainly blowing from right to left on the figure.

We clearly observe the decrease of humidity with height. The air above the middle part of the field has much more water vapor than the surrounding areas.

Smaller scans were acquired during the same sunny afternoon. One of them is shown in Fig. 9. A faster scan allows us to catch almost instantaneous behavior of water vapor.

It clearly shows the internal boundary layer shape due to the wind and the roughness

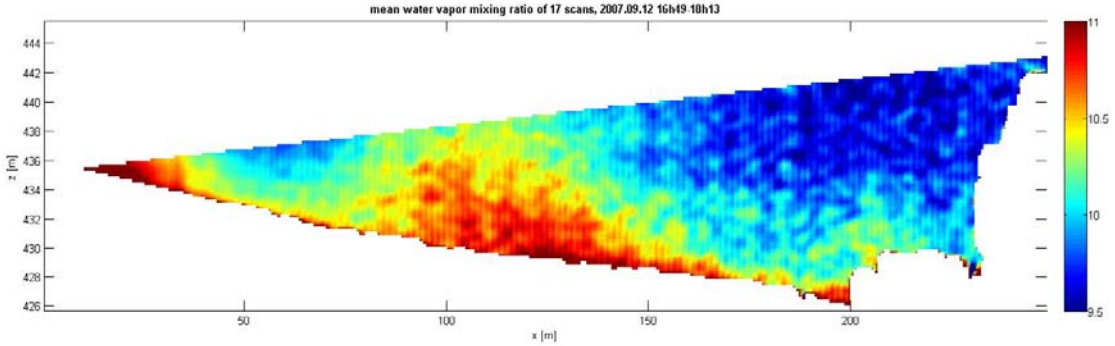

Figure 8. Mixing ratio vertical scan

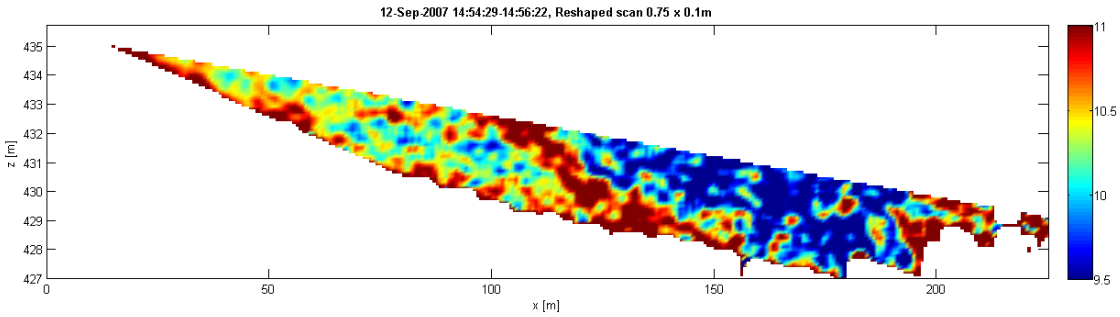

Figure 9. Mixing ratio small vertical scan

change at the end of the vineyard, at 180 m from the lidar. The difference between dry air coming on the site and the more humid air above the field is evident and is about 1 g/kg.

Conclusion

The EPFL water vapor and temperature Raman lidar design has been proven to be valid. The accuracy of the measurements that we obtained during the vineyard test field campaign is promising. The lidar can mesure turbulent structures of meter in size (or less during scans) and over time periods of seconds. Although it was not possible to observe one structure clearly associated with the surface in the horizontal scans, internal boundary shape at the vineyard edge was observed in the vertical scans. Ongoing research investigates methods to derive fluxes of water and heat directly from vertical scans. With such tools, we have now the capacity to measure surface-atmosphere exchanges of water vapor and heat at small scales, which is crucial for the characterization of evaporation and heat fluxes variability and dynamics (Parlange, Eichinger et al. 1995). The question of the spatial footprint of point sensors can be also addressed.

References

Arshinov, Y. F., S. M. Bobrovnikov, *et al*. (1983). Atmospheric-temperature measurements using a pure rotational raman lidar. *Applied Optics* **22(19)**, 2984-2990.

Grant, W. B. (1991). Differential absorption and raman lidar for water-vapor profile measurements - a review. *Optical Engineering* **30(1)**, 40-48.

Mattis, I., A. Ansmann, *et al*. (2002). Relative-humidity profiling in the troposphere with a Raman lidar. *Applied Optics* **41(30)**, 6451-6462.

Parlange, M. B., W. E. Eichinger, *et al*. (1995). Regional-scale evaporation and the atmospheric boundary-layer. *Reviews of Geophysics* **33(1)**, 99-124.

Renaut, D., J. C. Pourny, *et al*. (1980). Daytime raman-lidar measurements of water-vapor." *Optics Letters* **5(6)**, 233-235.

Whiteman, D. N., S. H. Melfi, *et al*. (1992). Raman lidar system for the measurement of water-vapor and aerosols in the earths atmosphere. *Applied Optics* **31(16)**, 3068-3082**.**